

Novel subjet observables for jet quenching in heavy-ion collisions

Liliana Apolinário^{1,2a}, José Guilherme Milhano^{1,2,3b}, Mateusz Ploskon^{4c}, and Xiaoming Zhang^{5d}

¹ LIP, Av. Prof. Gama Pinto, 2, 1649-003 Lisbon, Portugal

² IST University of Lisbon, Av. Rovisco Pais 1, 1049-001, Lisbon, Portugal

³ Theoretical Physics Department, CERN, CH-1211, Geneva 23, Switzerland

⁴ Lawrence Berkeley National Laboratory, Berkeley, California 94720, USA

⁵ Institute of Particle Physics, Central China Normal University, Wuhan 430079, China

Received: date / Revised version: date

Abstract. Using a novel observable that relies on the momentum difference of the two most energetic subjets within a jet ΔS_{12} we study the internal structure of high-energy jets simulated by several Monte Carlo event generators that implement the partonic energy-loss in a dense partonic medium. Based on inclusive jet and dijet production we demonstrate that ΔS_{12} is an effective tool to discriminate between different models of jet modifications over a broad kinematic range. The new quantity, while preserving the collinear and infrared safety of modern jet algorithms, it is experimentally attractive because of its inherent resilience against backgrounds of heavy-ion collisions.

PACS. 12.38.Mh Quark-gluon plasma – 13.87.-a Jets in large- Q^2 scattering – 24.10.Lx Monte Carlo simulations – 25.75.-q Relativistic heavy-ion collisions

1 Introduction

Interactions of high-energy partons with a strongly coupled hot partonic medium - a quark-gluon plasma (QGP) [1–4] - created in heavy-ion collisions, leading to modifications of the internal jet structure (jet quenching), was first proposed in [5] and is studied as a sensitive probe of the medium properties [6–8]. Experiments at RHIC and the LHC observed a strong suppression of high transverse momentum particle yields [9–15], suppression of inclusive and semi-inclusive yields of fully reconstructed jets [16–20], and, more recently, the internal structure of the jets [21–25] for detailed studies of jet quenching. However, in all these measurements the treatment of the background originating from the copiously produced particles not associated to hard scatterings poses an experimental challenge for precise and unbiased measurements. Previous works that addressed the effect of filtering on subjet analysis [26] and the recent analytic calculations of the momentum distributions of subjets [27–29] and groomed jet mass distributions [30–32] that were recently measured in proton-proton collisions [33,34], provide a strong motivation for novel studies. In this writeup, following previous works [35], we propose observables that are sensitive to the internal jet structure but significantly alleviate the difficulties associated to the effects of the background. Our

approach is attractive from the experimental point of view and obeys the theoretical requirements of the infrared and collinear safety.

While jet substructure techniques are extensively used in the high-energy pp collisions [36–38] the first studies in the heavy-ion context [24,39] are recent (see [35] for a first attempt of using subjets as a phenomenological tool for jet quenching studies). In this manuscript we propose an observable that uses only the highest and next-to-highest energetic fully reconstructed subjets within a jet. This choice aims to minimize the impact of the heavy-ion background on the extracted jet properties allowing for better experimental control.

2 Observable definition and setup

We introduce a new jet substructure observable ΔS_{12} defined as the difference between the fractions of transverse momentum of a jet carried by its leading (hardest) and subleading (second hardest) subjets. That is

$$\Delta S_{12} = z_1 - z_2, \quad (1)$$

where

$$z_i = p_{T,i}/p_{T,\text{jet}}. \quad (2)$$

The subjets used to evaluate eq. (1) are obtained as follows:

1. For each event, reconstruct jets with the anti- k_T algorithm [40] provided by the FASTJET package [41] with radius R and within pseudo-rapidity $|\eta_{\text{jet}}| < \eta_{\text{max}}$;

^a liliana@lip.pt

^b guilherme.milhano@ist.utl.pt

^c mploskon@lbl.gov

^d xiaoming.zhang@cern.ch

2. Within each jet, find subjets by reclustering the jet components with a smaller radius parameter $R_{\text{sj}} < R$. Retain the two hardest (highest- p_T) subjets.

The subjet samples used in this study were obtained with $\eta_{\text{max}} = 2.5$ and $R = 0.5$. In general, the reclustering of the jet components into subjets in step (ii) above can be carried out with a different jet algorithm from that chosen to reconstruct the jet to which they belong. We chose to use anti- k_T after assessing the discriminating power of ΔS_{12} for subjets reconstructed with different algorithms and checking its sensitivity to hadronization effects (see Subsections 4.2 and 4.4). The subjet radius parameter was set to $R_{\text{sj}} = 0.15$ except when assessing, in Subsection 4.2, the dependence of ΔS_{12} on R_{sj} (where the range $0.1 < R_{\text{sj}} < 0.2$ was considered), and when comparing, in Subsection 4.5, with the analysis [24] (where we used $R_{\text{sj}} = 0.1$).

The bulk of soft particles produced in high-energy collisions is not a priori distinguishable from the particles produced from the hadronisation of an energetic parton shower. The presence of these background particles is the main experimental confounding factor when establishing the jet energy scale and jet energy resolution in jet quenching studies (see for example [42]). Moreover, unlike in measurements of proton-proton collisions with high event pile-up probability within the detectors, the background in heavy-ion collisions is complex. It consists of region to region fluctuations, modified particle production as compared to pp collisions, and particle correlations caused by the collective expansion of the QGP. In consequence, experimental observables at relatively low jet energies at the LHC ($p_T < 150$ GeV) are prone to systematic uncertainties related to complicated multi-dimensional unfolding procedures that are susceptible to large correction factors.

The substructure observable ΔS_{12} defined in eq. (1) has been constructed to minimize correlated background contributions. Take [43]

$$\Delta S_{12} = \frac{p_{T,1}^{\text{true}} - p_{T,2}^{\text{true}}}{p_{T,\text{jet}}} = \frac{(p_{T,1}^{\text{rec}} - \rho_1 A_1) - (p_{T,2}^{\text{rec}} - \rho_2 A_2)}{p_{T,\text{jet}}}, \quad (3)$$

where $p_{T,i}^{\text{true}}$ is the true subjet momentum, A_i is the area of a subjet, ρ_i is the level of noise corresponding to the amount of transverse momentum added to each subjet per unit area by the background, and the $p_{T,i}^{\text{rec}}$ is the experimentally reconstructed subjet momentum containing the background contribution $\rho_i A_i$. For subjets reconstructed with the same radius parameter R_{sj} (in our case $R_{\text{sj}} = 0.15$) with the anti- k_T algorithm, the corresponding active areas are necessarily very similar $A_1 \simeq A_2$. In an ideal case, where $\rho_1 = \rho_2$, the background term in the numerator of ΔS_{12} vanishes. For real events, where subjets sit close by, ρ_1 and ρ_2 can only differ by very localized fluctuations and thus should be on average still very similar. Thus, the background effect in the numerator of eq. (1) is small.

A variety of observables similar to ΔS_{12} can be defined. In particular, z_i in eq. (2) could be redefined by replacing the denominator by the sum of the momenta of the leading

and subleading subjets, such that $z_i = p_{T,i}/(p_{T,1} + p_{T,2})$. Although such a definition could have some welcome consequences in reducing the influence of background effects in the reconstructed jet transverse momentum $p_{T,\text{jet}}$ (denominator of eq. 2), all information on the overall hardness of the jet fragmentation, that is the fraction of jet momentum carried by the two hardest subjets, would be neglected.

3 Models

To assess the potential of the proposed observable we consider a set of Monte Carlo event generators which rely on different implementations of jet quenching. This allows both for a comparison between theoretical calculations that is not limited by systematic uncertainties of the putative experimental measurement and to assess the potential of the observable as a discriminant of different modelling scenarios.

Below we provide a short description of each event generator considered in this study — Q-PYTHIA v1.0.2 [44], JEWEL v2.0.0 [45], and PYQUEN v1.5.1 [46] — emphasising only the main characteristics and details of the setup we adopted (for further details please see the corresponding references). All samples used in this work were generated for central (0-10% most central) PbPb collisions at $\sqrt{s_{NN}} = 2.76$ TeV.

Q-PYTHIA is a modification of PYTHIA 6.4 [47] where the splitting probability in the final state parton shower is enhanced by an additional term that follows the BDMPS-Z radiation spectrum [48]. The medium is modelled by a single parameter, a local in space and time transport coefficient \hat{q} that translates the averaged transverse momentum squared $\langle q_T^2 \rangle$ exchanged between a parton and the medium per mean free path λ in that medium, such that $\hat{q} = \langle q_T^2 \rangle / \lambda$. The time and spatial variation of \hat{q} is modelled following the PQM prescription [49]. We considered two different average \hat{q} values ($\hat{q} = 1 \text{ GeV}^2 \text{ fm}^{-1}$ and $\hat{q} = 4 \text{ GeV}^2 \text{ fm}^{-1}$) known to capture the main jet quenching features observed in dijets [50].

JEWEL implements a description of jet evolution that takes into account both elastic and inelastic energy losses as all scatterings with the medium are described by infrared continued leading order matrix elements for $2 \rightarrow 2$ processes. Additional medium-induced radiation is also taken into account during the jet development and can be induced by several coherent scatterings, as predicted by the LPM effect [51, 52]. We kept all default settings and used the medium implementation with Bjorken expansion described in detail in [53] validated on a large set of jet quenching observables [45].

PYQUEN is a modification (afterburner) of standard PYTHIA 6.4 jet events in which both radiative and collisional accumulated energy losses are applied during the parton shower development. The former is calculated for an expanding medium within the BDMPS framework, where the angular distribution follows three simple parameterisations (small, wide and collinear angular distributions)

that are used for comparison purposes. The latter is calculated in the high-momentum transfer approximation. Additional in-medium gluon radiation is added at the end of the parton shower, before hadronization. We chose the internal parameters that characterise the QGP formation expected for central PbPb collisions at the LHC.

While a typical Monte Carlo reference for jet production in pp collisions is constructed with PYTHIA [47] each of the models provides their own implementation and/or modifications of PYTHIA original routines and consequently their own pp reference. Therefore, when comparing the medium-modified jets with jets showering in vacuum we take the model-provided proton-proton collision equivalent.

4 Results

We provide examples of how ΔS_{12} can be used to discriminate between the different implementations of jet quenching (Sec. 4.1) and evaluate its sensitivity to the choice of algorithm for subjet clustering and subjet radius R_{sj} (Sec. 4.2). Section 4.3 illustrates how ΔS_{12} combined with a dijet analysis can be used to study jet quenching more differentially as compared to the inclusive measurements. In section 4.4 we show the robustness of the results against hadronization effects. Finally, Sec. 4.5 provides an overview of the relation between ΔS_{12} and the recently explored z_g observable in vacuum.

4.1 ΔS_{12} as a model discriminant

The distribution of the difference ΔS_{12} between the fractions of the jet total transverse momentum carried by the leading and subleading subjets is shown in Figure 1.

In vacuum – Q-PYTHIA (vac) and JEWEL (vac) (top panel), and PYTHIA 6 (bottom panel) – the distribution displays a pronounced maximum for $\Delta S_{12} > 0.9$ and a tail towards lower ΔS_{12} values. Medium effects in Q-PYTHIA and JEWEL (top panel) modify the ΔS_{12} distribution in incompatible directions. JEWEL enhances significantly the maximum of the distribution and mildly depletes its tail. Q-PYTHIA softens the peak at high ΔS_{12} and produces a flat tail towards values of $\Delta S_{12} \leq 0.7$ with the effects more pronounced for increasing \hat{q} . These observations are consistent with a collimation of jets in JEWEL and broadening in Q-PYTHIA as compared to their vacuum references. PYQUEN (Coll) (bottom panel) modifies the ΔS_{12} similarly to JEWEL, PYQUEN (Small) gives a distribution with features resembling those found for Q-PYTHIA, and PYQUEN (Wide) displays an intermediate behaviour.

While the above features directly reflect the behaviour of the z_1 and z_2 distributions (see appendix A), we emphasise that, from the experimental point of view, studies of ΔS_{12} are more attractive as compared to the individual z_i distributions since the difference $z_1 - z_2$ removes, by construction, a large fraction of the correlated background. Although the effect of the uncorrelated background is enhanced in ΔS_{12} ratio with respect to z_2 on a jet-by-jet

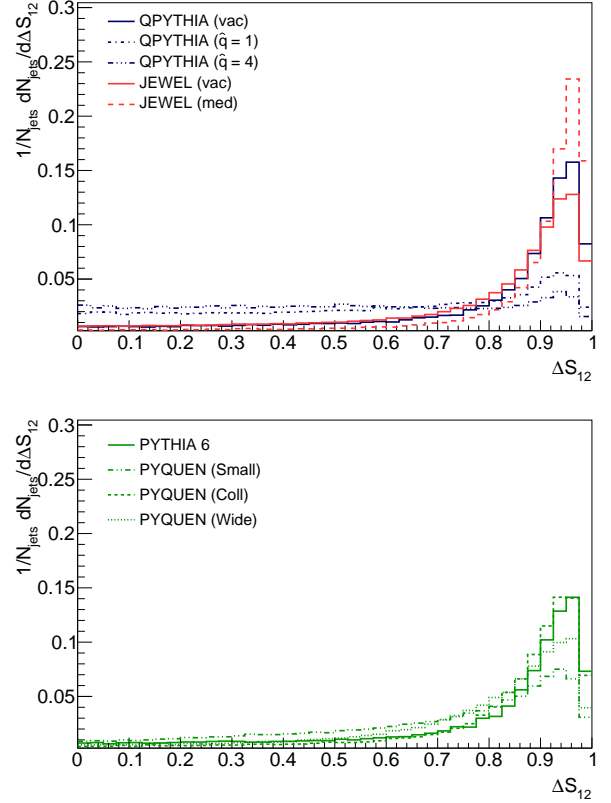


Fig. 1. Distribution of ΔS_{12} for $R_{sj} = 0.15$ anti- k_T subjets within $R = 0.5$ anti- k_T jets with $p_T > 150$ GeV/ c .

basis, we found that this effect is small when taking the integrated/inclusive distributions, and subsequently their moments. Moreover, ΔS_{12} is more robust for low momentum jets for which z_2 becomes gradually (with decreasing p_T) dominated by background particles. u

To further expose the differences among models we now turn our focus to the quartiles of the ΔS_{12} distribution, considering *med/vac* ratios \mathcal{R} , where *med* refers to calculations including jet quenching effects and *vac* to the corresponding model specific no-quenching baseline

$$\mathcal{R}_{Q_i[\Delta S_{12}]} = \frac{Q_i[\Delta S_{12}]^{med}}{Q_i[\Delta S_{12}]^{vac}}. \quad (4)$$

While the *med/vac* ratio of the medians of the ΔS_{12} distributions as a function of p_T^{jet} display a clear evolution and discrimination power among the models (data not shown), we find that to characterise the modifications to the subjet structure for models that show jet collimation – JEWEL and PYQUEN (Coll) – the ratios of the first quartile (Q_1) of ΔS_{12} distributions is preferable. The criteria of selecting the *best* discriminant was made by calculating the relative standard deviation (RSD) given by the models in each p_T bin, i.e, the ratio of the standard deviation over the mean. The relative spread among the different models for each observable is thus quantified (a larger spread translates into a larger RSD) and it can be

used as a guiding parameter to select the observable that maximizes the differences among jet quenching models.

The ratios $\mathcal{R}_{Q_1[\Delta S_{12}]}$ are shown in Figure 2, in the upper panel, while the corresponding RSD in the bottom panel of the same figure.

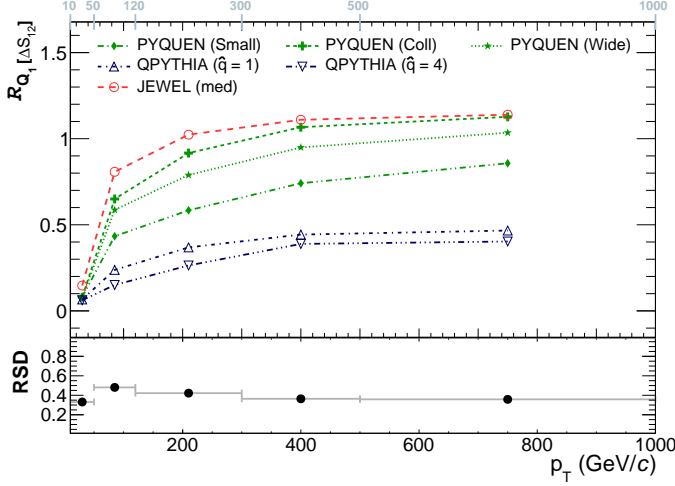


Fig. 2. *Top panel:* $\mathcal{R}_{Q_1[\Delta S_{12}]}$ as a function of p_T^{jet} ; *Bottom panel:* RSD of $\mathcal{R}_{Q_1[\Delta S_{12}]}$ as a function of p_T^{jet} . The edges of the five considered jet p_T bins (10-50, 50-120, 120-300, 300-500, 500-1000 GeV/c) are shown on the top of the figure.

Here we find a clear evolution with the jet momentum for jets with $p_T < 300$ GeV/c for all models. Up to this jet p_T all models show a suppression of $\mathcal{R}_{Q_1[\Delta S_{12}]}$ reflecting more balanced momentum sharing between the two leading subjet structures than in the vacuum references. However, at high jet p_T , this observable remains fairly constant and shows a strong sensitivity to models that produce jets with a more symmetric structure, such as Q-PYTHIA and PYQUEN(Small) ($\mathcal{R}_{Q_1[\Delta S_{12}]} < 1$) separating them well apart from PYQUEN (Wide and Coll) and JEWEL ($\mathcal{R}_{Q_1[\Delta S_{12}]} \simeq 1$).

Further, we find that the interquartile range IQR = $Q_3 - Q_1$, that characterises the *width* of the ΔS_{12} distribution, gives additional information. Figure 3 shows $\mathcal{R}_{IQR[\Delta S_{12}]}$ as a function of jet transverse momentum for the different quenching models with the corresponding RSD calculated in each p_T bin. Here again, models that result in jet collimation, characterised by a similar or narrower ΔS_{12} distribution than its vacuum reference ($\mathcal{R}_{IQR[\Delta S_{12}]} \leq 1$), are clearly separated from those that broaden the jet, where ΔS_{12} is typically broader with respect to the vacuum reference ($\mathcal{R}_{IQR[\Delta S_{12}]} > 1$).

Moreover, for Q-PYTHIA, JEWEL and PYQUEN(Coll), $\mathcal{R}_{IQR[\Delta S_{12}]}$ converges quickly to a constant value with increasing jet p_T . Importantly, it also allows to better discriminate between the two models that destroy the vacuum subjet asymmetry: while Q-PYTHIA is well separated from its vacuum reference for all $p_T > 100$ GeV/c, PYQUEN(Small) evolves slowly towards more asymmetric jets with increasing p_T . Thus, $\mathcal{R}_{IQR[\Delta S_{12}]}$ provides relevant

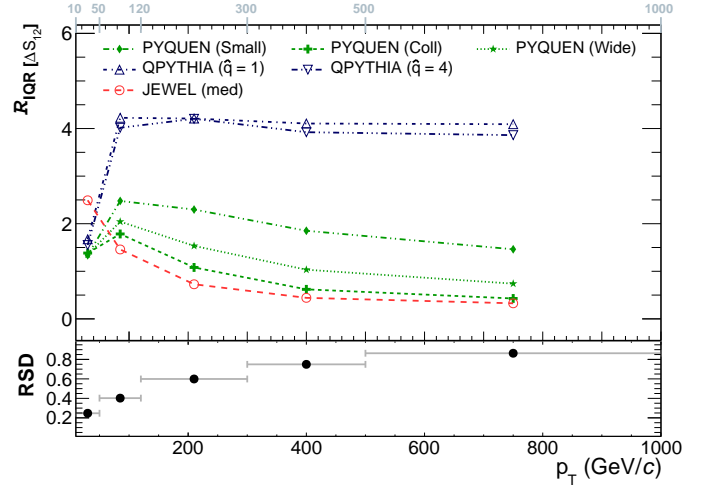


Fig. 3. *Top panel:* $\mathcal{R}_{IQR[\Delta S_{12}]}$ as a function of p_T^{jet} ; *Bottom panel:* RSD of $\mathcal{R}_{IQR[\Delta S_{12}]}$ as a function of p_T^{jet} . The edges of the five considered jet p_T bins (10-50, 50-120, 120-300, 300-500, 500-1000 GeV/c) are shown on the top of the figure.

complementary information to identify the main characteristics of jet quenching within specific models, in particular for jets with $100 < p_T < 200$ GeV/c, where the first quartile Q_1 of the ΔS_{12} is suppressed with respect to the vacuum reference in all models. Comparing the RSD of $\mathcal{R}_{Q_1[\Delta S_{12}]}$ and $\mathcal{R}_{IQR[\Delta S_{12}]}$ we find that for low p_T jets (jets with $p_T < 120$ GeV/c), the $\mathcal{R}_{Q_1[\Delta S_{12}]}$ has a higher discrimination power while $\mathcal{R}_{IQR[\Delta S_{12}]}$ is preferable for higher p_T jets. Nonetheless, it should be noted that IQR is also more sensitive to hadronization effects (see section 4.4)

We also investigated the evolution of ΔS_{12} with the relative distance ΔR_{subjet} in (η, ϕ) space between the leading and subleading subjets, in particular of the *med/vac* of its median value Q_2 and interquartile range IQR. The corresponding RSD are calculated in each ΔR_{subjet} bin.

The median ratio (Figure 4) shows a clear separation between models – Q-PYTHIA and PYQUEN(Small) – that broaden the jet structure. In Q-PYTHIA the two leading subjets become more symmetric with increasing ΔR_{subjet} (the ratio is below one and decreases). The same behaviour is seen for PYQUEN(Small) up to $\Delta R_{\text{subjet}} = 0.25$, but interestingly, vacuum-like behaviour is recovered for larger separations. In contrast, the median ratio in JEWEL and PYQUEN(Coll) show a dependence on ΔR_{subjet} similar to their vacuum references with the ratio nearly independent of the distance between the two leading subjets. The large reduction of the interquartile range ($\mathcal{R}_{IQR[\Delta S_{12}]} < 0.5$) for all ΔR_{subjet} observed (Figure 5) in these models provides another clear signature of the jet collimation effect.

From the RSD values the interquartile ratio allows to have a wider spread between the models, although the transition from PYQUEN(Small) to vacuum-like behaviour is more noticeable through the median ratio.

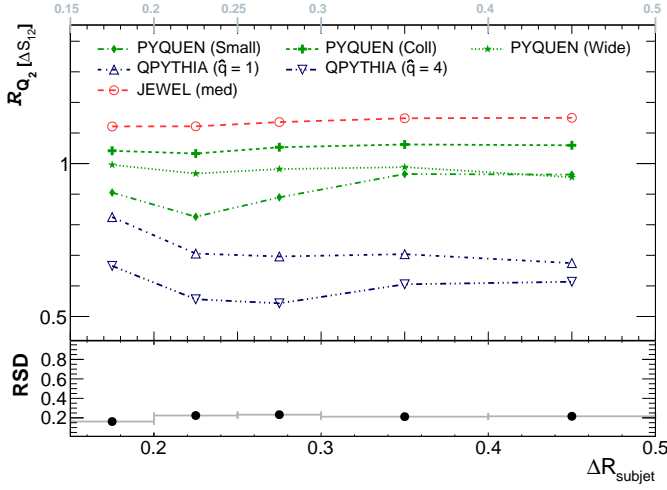


Fig. 4. *Top panel:* $R_{Q_2[\Delta S_{12}]}$ as a function of ΔR_{subjet} ; *Bottom panel:* RSD of $R_{Q_2[\Delta S_{12}]}$ as a function of ΔR_{subjet} . The edges of the five considered ΔR_{subjet} bins: (0.15-0.2; 0.2-0.25; 0.25-0.3; 0.3-0.4; 0.4-0.5) are shown on the top of the figure.

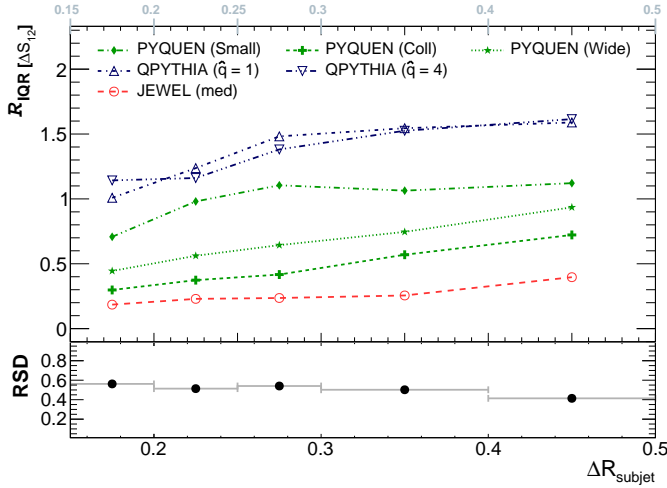


Fig. 5. *Top panel:* $R_{IQR[\Delta S_{12}]}$ as a function of ΔR_{subjet} ; *Bottom panel:* RSD of $R_{IQR[\Delta S_{12}]}$ as a function of ΔR_{subjet} . The edges of the five considered ΔR_{subjet} bins: (0.15-0.2; 0.2-0.25; 0.25-0.3; 0.3-0.4; 0.4-0.5) are shown on the top of the figure.

4.2 Dependence on the choice of subjet clustering algorithm and subjet radius

To investigate the dependence of the proposed observable and its sensitivity to the effects of jet quenching we varied the subjet reconstruction algorithm as well as the subjet radius parameter $R_{sj} < R$.

We find no significant differences in ΔS_{12} subjet distributions when changing the clustering algorithm from anti- k_T [40] to k_T [54] or Cambridge-Aachen (C/A) [55]. However, ΔR_{subjet} depends, by construction, on the reconstruction algorithm. Figure 6 shows the *med/vac* ratio of the medians of ΔR_{subjet} distributions for different models for $p_T > 150$ GeV/c jets with the subjet radius set, as before, to $R_{sj} = 0.15$, and the corresponding RSD for completeness. The integer values -1, 0, 1 on the x-axis

correspond, respectively, to anti- k_T , C/A, and k_T . Despite the finite differences between clustering algorithms, we find that the power of discrimination between the different models is largely independent of the choice of the algorithm. This observation, together with the results obtained in section 4.4, where we study the effect of different hadronization models on the reconstructed subjets, allow us to conclude that the anti- k_T algorithm provides the most promising option when optimising for jet quenching effects. We therefore adopt this clustering algorithm as the standard setting for the remainder of this work.

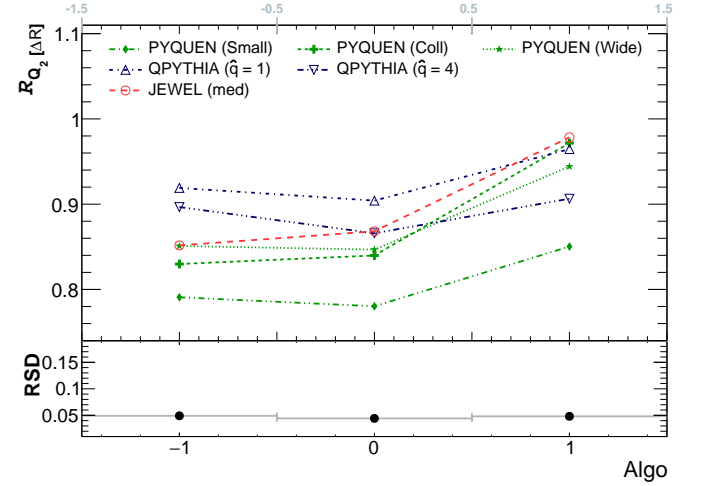


Fig. 6. Evolution of the *med/vac* ratio of the medians of ΔR distributions $R_{Q_2[\Delta R]}$ (*top panel*) and corresponding RSD (*bottom panel*) with the subjet reconstruction algorithm with radius of $R_{sj} = 0.15$ for anti- k_T jets with $p_T > 150$ GeV/c.

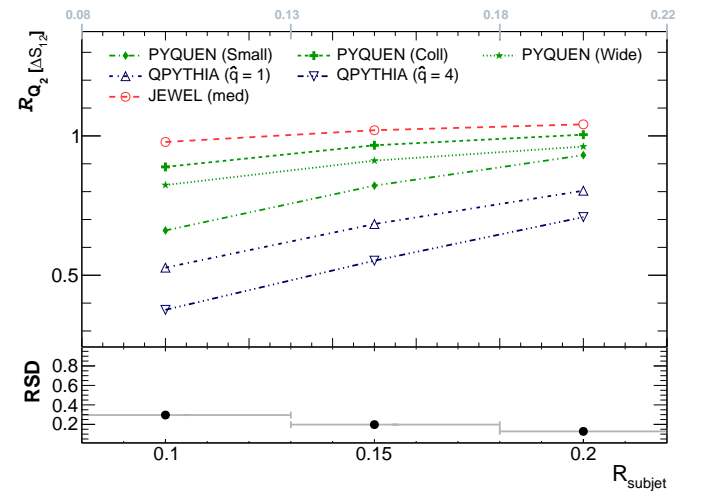


Fig. 7. Evolution of the *med/vac* ratio of the medians of ΔS_{12} distributions $R_{Q_2[\Delta S_{12}]}$ (*top panel*) and corresponding RSD (*bottom panel*) with the subjet radius R_{sj} for anti- k_T jets with $p_T > 150$ GeV/c.

Figure 7 shows the dependence on R_{sj} of the *med/vac* ratio of the medians of ΔS_{12} distributions for subjets reconstructed with the anti- k_T algorithm. The RSD is also shown in the bottom panel, now calculated for each algorithm separately. Here, we find that an increased discrimination between models resulting in jet collimation and the models preferring jet broadening is achieved with $R_{\text{sj}} \in [0.1; 0.15]$. Further, we find a clear difference in the energy distribution inside the jet that results from the different models. On the one hand, Q-PYTHIA and PYQUEN(Small) increase the leading subjet p_T when the subjet radius is increased, indicating broadening of the jet structure. On the other hand, in the models that produce collimated jets by medium effects, the energy in the leading subjet is nearly independent of the chosen subjet radius as it is highly concentrated close to the jet core.

4.3 Subjets in dijet pairs

In a back-to-back dijet pair propagating through the QGP, the sub-leading jet has typically lost more energy than its leading partner [56]. This quenching asymmetry can be combined with ΔS_{12} to experimentally further constrain the nature of jet quenching. We have performed an analysis of dijet pairs with $R = 0.5$ anti- k_T jets within with $|\eta_{\text{jet}}| < 2$ where the leading jet was required to have $p_T > 120$ GeV/c and the recoil jet $p_T > 50$ GeV/c. The jets in the pair were required to be separated in azimuth by at least $5/6\pi$. The *med/vac* ratios of medians of the ΔS_{12} distribution, $\mathcal{R}_{Q_2[\Delta S_{12}]}$, as a function of $x_J = p_T^{\text{recoil jet}} / p_T^{\text{leading jet}}$ are shown in Figure 8. The upper figures show results for leading jets and the bottom figures those for recoil jets. Again, the upper panels of each figure show the evolution of all models and the bottom panels the corresponding spread quantified through the RSD calculated in each asymmetry bin.

Models that collimate jets towards their core – JEWEL and PYQUEN (Coll) – display leading jets with a (slightly) enhanced asymmetric subjet momentum balance as compared to their vacuum references, while the recoil jets have a more balanced subjet momentum distribution than in vacuum. In contrast, in models that broaden the jet structure – Q-PYTHIA, PYQUEN (Small), and to a more limited extent PYQUEN (Wide) – both leading and recoil jets have a more balanced subjet momentum distribution than in vacuum with the modification significantly stronger for recoil jets. In all cases, the leading jet is modified independently of the pair asymmetry, while the momentum sharing between subjets becomes increasingly balanced (with respect to vacuum) with increasing dijet asymmetry (decreasing x_J) for recoil jets.

Similar findings are also present in the ratio of the interquartile range of the distributions, for both leading and recoil jets, shown in Fig. 9. However, differences between leading jets are more noticeable through the asymmetry of the ΔS_{12} distribution while recoil jets show a larger spread among models through $\mathcal{R}_{Q_2[\Delta S_{12}]}$.

All these observations are consistent with the findings from section 4.1, figure 2, where jets below $p_T =$

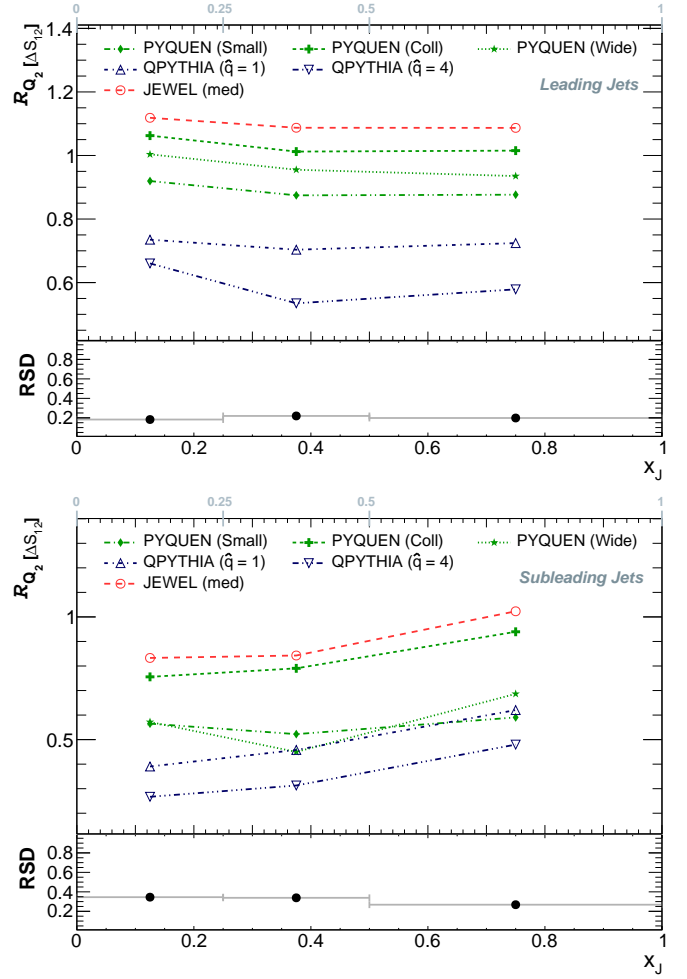


Fig. 8. $\mathcal{R}_{Q_2[\Delta S_{12}]}$ as a function of x_J for (*top figure*) leading jets and (*bottom figure*) recoil jets in dijet pairs. The edges of the three considered x_J bins (0-0.25; 0.25-0.5; 0.5-1) are shown on the top of the figure. The bottom panel of each figure show the corresponding RSD.

200 GeV/c always have a ΔS_{12} that is smaller than its vacuum reference. This is the preferred kinematic region for the recoil jet in unbalanced dijet systems. Moreover, $\mathcal{R}_{Q_1[\Delta S_{12}]}$ is fairly constant for jets above $p_T = 200$ GeV/c, where the leading jet (and recoil for balanced dijet systems) typically comes.

4.4 Hadronization effects on the reconstructed subjets

Small radii jets are known to be more sensitive to hadronization effects [57]. For this reason, we investigate the role of different hadronization models in the distributions that were presented so far by using both PYTHIA 8 and HERWIG 7 [58, 59]. The former is based solely on the Lund string fragmentation framework [60] while the later applies a cluster model [61] to hadronize the resulting partonic final state to produce hadrons. Although such study is not ideal to accurately assess the uncertainties induced by hadronization effects, including in-medium hadroniza-

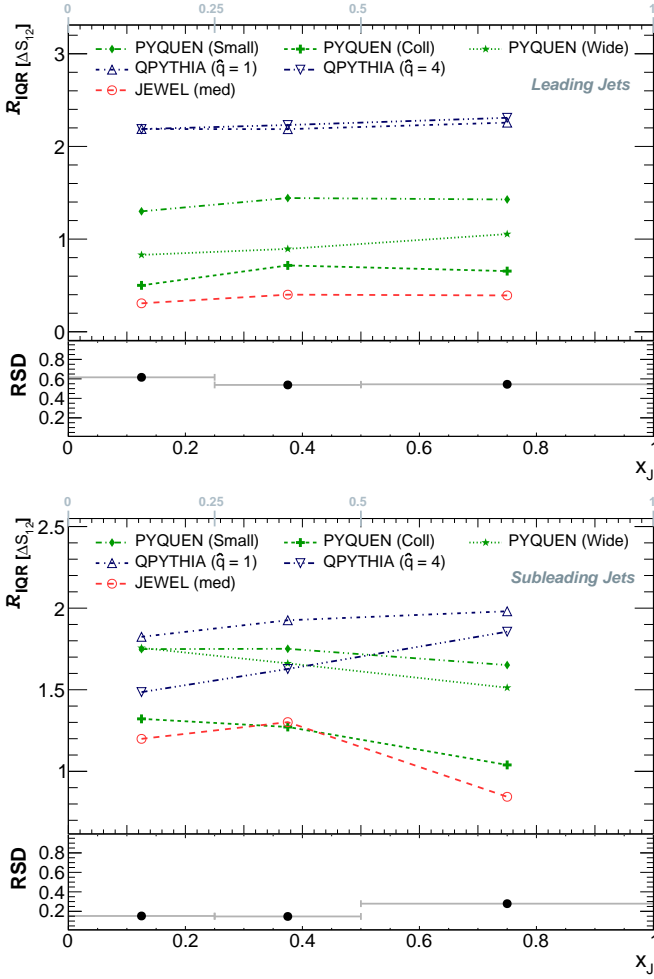


Fig. 9. $\mathcal{R}_{\text{IQR}}[\Delta S_{12}]$ as a function of x_J for (top figure) leading jets and (bottom figure) recoil jets in dijet pairs. The edges of the three considered x_J bins (0-0.25; 0.25-0.5; 0.5-1) are shown on the top of the figure. The bottom panel of each figure show the corresponding RSD.

tion modifications [62], it can provide an estimate of the robustness of the proposed observable, ΔS_{12} .

We have found that $Q_2[\Delta S_{12}]$ is almost insensitive to the hadronization model, with relative differences (taking PYTHIA 8 as reference) smaller than 1% for any choice of subjet radius or clustering algorithm and jets with a transverse momentum $p_{T,jet} > 100$ GeV/c. For low momentum jets ($p_{T,jet} < 100$ GeV/c), this difference goes up to 2% for $R_{subjet} = 0.15$ and 10% for $R_{subjet} = 0.1$.

As for the first quartile of the distribution, $Q_1[\Delta S_{12}]$, the relative change of HERWIG 7 with respect to PYTHIA 8 is $\sim [2 - 5]\%$ for anti- k_T subjets with $R_{subjet} \leq 0.15$. Any other choice of clustering algorithm or subjet radius provide a relative difference of $\sim [5 - 10]\%$ independently of the jet transverse momentum.

Finally, the interquartile range, $\text{IQR}[\Delta S_{12}]$ that is able to provide, in general, a larger dispersion between the jet quenching models, is also able to discriminate more among hadronization models. The relative change in low momen-

tum jets ($p_{T,jet} < 100$ GeV/c) between the interquartile range provided by the two Monte Carlo event generators is around $[4 - 10]\%$ for any clustering algorithm and subjets reconstructed with $R_{subjet} \leq 0.15$. For $R_{subjet} = 0.2$, this change increases to 17%, independently of the clustering algorithm. In high momentum jets ($p_{T,jet} > 250$ GeV/c) the relative difference is around $[20 - 40]\%$. The lower bracketing is constantly observed for anti- k_T and small radius subjets while the upper bracketing occurs for k_T and large radius subjets. For the chosen parameters of this manuscript (anti- k_T subjets with $R_{subjet} = 0.15$), the relative change is $\sim 25\%$ for any jet with $p_{T,jet} > 100$ GeV/c.

The general large sensitivity of the interquartile range to the choice of the hadronization model comes from the fact that this observable is designed to promote the tails of the distributions. While it is the preferable region to tag energy loss modifications imprinted on the jet, it is also the region dominated by a fragmentation pattern that promotes the existence of one ($\Delta S_{12} \sim 1$) or two ($\Delta S_{12} \sim 2$) subjets mainly composed by very soft particles. Any modification on the hadronization mechanism would imply a stronger deviation on both $Q_1[\Delta S_{12}]$ (as observed from the increase of the relative differences with respect to $Q_2[\Delta S_{12}]$) and $Q_3[\Delta S_{12}]$.

These observations validate our choice of using reclustered anti- k_T subjets with $R_{subjet} = 0.15$ as to maximize jet quenching phenomena with respect to hadronization effects.

4.5 Sub-jet momentum fraction z_g and ΔS_{12}

Recent studies of the momentum fraction z_g in jets [24] prompt for a comparison of z_g with ΔS_{12} . We have performed an analysis of (vacuum) PYTHIA jets with $p_T > 150$ GeV/c using settings of the SOFT DROP algorithm [63, 64] as in [24]. Figure 10 shows the z_g as a function of ΔS_{12} for two cases: one, where all jets were used; and a second, where jets with $\Delta R_{sj} < 0.1$ between the subjets used to calculate z_g are discarded. ΔS_{12} was calculated with $R_{subjet} = 0.1$ in both cases. We find a strong correlation between ΔS_{12} and the calculation of z_g when using the ΔR_{sj} cut as in [24]. Without the cut on ΔR_{sj} the distributions have two dominating structures. One is the diagonal, but the other is largely independent of the ΔS_{12} at $\Delta S_{12} > 0.8$.

A comment on the differences of behaviour between these two observables in the presence of a QGP is in order. One of the proposed explanations [65] for the observed modification of the z_g distribution in nucleus-nucleus collisions relies on the ability of subjets to collect contributions from the QGP. As argued in that work, this QGP backreaction process implies a distinctive increase in size (measured girth) of the subjets. Since in ΔS_{12} we explicitly impose, by specifying a radius parameter R_{sj} for the subjet reconstruction, a size for the subjets, contributions from the QGP to both subjets will be of the same order, and thus, will cancel in ΔS_{12} . This makes ΔS_{12} and z_g , well correlated in vacuum, complementary observables in the presence of a QGP that can be used to disentangle the

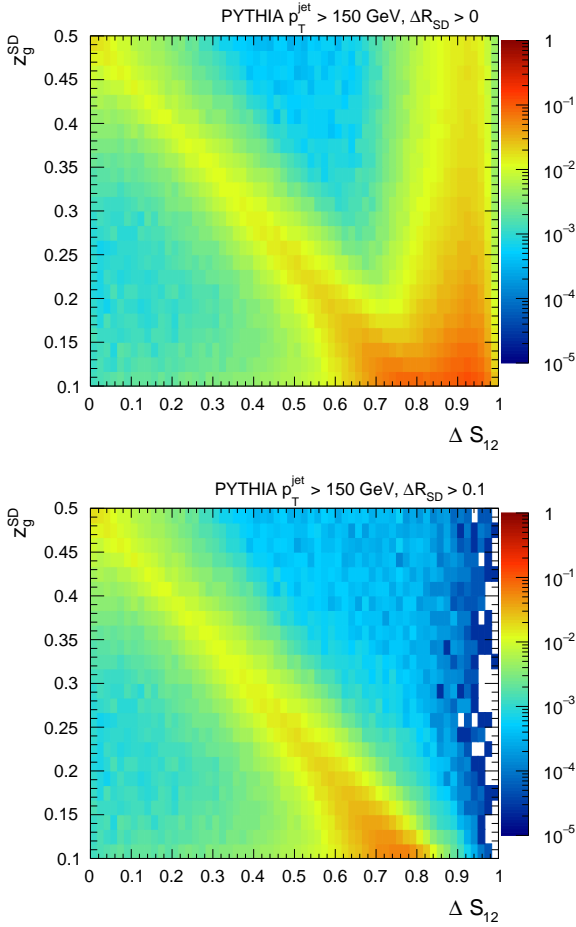


Fig. 10. Subjet momentum fraction z_g^{SD} reconstructed using the SOFT DROP algorithm as a function of ΔS_{12} . *Upper panel:* distribution for all jets with $p_T > 150$ GeV/c. *Lower panel:* distribution for jets for which subjets used for calculating z_g are separated by a distance of $\Delta R > 0.1$.

role of QGP backreaction from other dynamical processes that conceivably modify the jet substructure.

5 Discussion

JEWEL. Results from JEWEL are consistent with a *jet collimation* effect, i.e., most of the radiation is transported outside of the cone leaving the energy core of the jet almost unmodified with respect to the vacuum reference but in a narrower region of phase space. We note, that in this analysis we have used JEWEL in its “recoil-off” mode which discards the medium partons that interacted with the jet. In this way, the results are independent of the medium-response, whose impact was recently analysed in [65]. As a consequence, the ΔS_{12} is closer to unity for the medium modified jets and it does not change with the chosen subjet radius. Moreover, the comparison of properties of the leading and subleading jets from a dijet event shows that ΔS_{12} increases for the leading jets and decreases for the (more strongly medium-modified/low momentum)

subleading jet. This is an exclusive characteristic of the jet collimation phenomena and/or collisional energy loss as the same kind of behaviour is observed for PYQUEN(Coll). In this model, since $\theta_{rad} = 0$, all the energy that is lost outside of the cone is due to elastic energy loss.

Q-PYTHIA. In Q-PYTHIA, which is as an implementation of the BDMPS-Z spectrum (without account for destructive interferences), the emission rate is enhanced according to the quenching parameter \hat{q} leading to a large modifications of the jet inner core. As a consequence, the distribution with a maximum for $\Delta S_{12} > 0.9$ in vacuum shows a large tail to lower values due to in-medium interactions due to softening of the subjet spectrum (including the leading subjet). Such effect is visible for both leading and subleading jets. Moreover, the medium-induced gluon radiation is evenly distributed in phase space up to very large distances as ΔS_{12} mean value is constantly below the vacuum reference without a significant change for $\Delta R_{subjet} > 0.2$.

PYQUEN. PYQUEN considerations are centred around three angular distributions for the in-medium radiation spectrum. For PYQUEN(Small) the finite angle of the radiation ($\theta < 5^\circ$) enhances the substructure and the impact on ΔS_{12} is qualitatively similar to Q-PYTHIA. Nonetheless, a striking difference from this model with respect to Q-PYTHIA is the increasing asymmetry of the subjet structure when biasing the jet sample with $\Delta R_{subjets} > 0.3$. This could be due to the fact that since the radiation is displaced at a finite angle from the leading parton, the more the second hardest subjet is reconstructed away from the jet core, the less probable is to recover the energy. As such, the energy-momentum distribution inside of the jet is located at intermediate distances from the jet core in contrast to what happens in Q-PYTHIA. A similar, but much milder modification of ΔS_{12} is observed for PYQUEN(Wide). Since gluon radiation goes as $\sim 1/\theta$, the radiation is essentially kept near the core with few particles going to very large angles. This angular distribution is similar to the jet vacuum development, which makes this model undistinguishable from the vacuum reference for jets with a large transverse momentum and/or leading jets in dijet systems. On the other hand, the PYQUEN(Coll) mode, constrained to elastic energy loss only, affects mainly the softest jet constituents by such elastic collisions, whose energy is “absorbed” by the medium. As such, jets become more collimated, as it happens in JEWEL.

Considerations of the RSD distributions show that the $\mathcal{R}_{IQR}[\Delta S_{12}]$ carries the largest discrimination power for high- p_T jets, although there is an associated uncertainty of [10 – 25]% due to hadronization effects. For low- p_T jets ($p_T \lesssim 120$ GeV/c) and/or recoil-jets in dijet systems the use of the $\mathcal{R}_{Q_1}[\Delta S_{12}]$ and/or the median $\mathcal{R}_{Q_2}[\Delta S_{12}]$ may prove more advantageous, with hadronization uncertainties that are smaller than 5% for the chosen subjet parameters.

Finally, we reiterate that inclusive or semi-inclusive measurements of nuclear modification factor(s) for jets that fall within a range of ΔS_{12} (and $\Delta R_{subjets}$) can pro-

vide a rather straightforward insight into the properties of jet quenching (see [35] for example).

6 Conclusions

We have presented observables of subjet structure that by minimizing the impact of the particle backgrounds in heavy-ion collisions are advantageous from the experimental point of view. At the same time, the introduced ΔS_{12} quantity preserves the collinear and infrared safety of modern jet algorithms. Using a number of Monte Carlo jet quenching models we have demonstrated that ΔS_{12} distribution and $\Delta R_{subjets}$ can be used as a sensitive tool to discriminate between different quenching mechanisms. We have shown that it is possible to use the quartiles of those distributions, together with the widths and/or use of dijets to make an accurate assessment of the main jet quenching characteristics, in particular, to determine the angular structure of the medium-induced gluon radiation and to investigate further the role of collisional energy loss in the in-medium shower development.

Acknowledgements

The authors would like to thank to N. Armesto, M. Verweij and K. Zapp for useful discussions.

This work was supported in part by the U.S. Department of Energy, Office of Science, Office of Nuclear Physics, under contract DE-AC02-05CH11231 (MP, XZ) and by the Fundação para a Ciência e Tecnologia (Portugal) under contracts CERN/FIS-NUC/0049/2015, Investigador FCT - Development Grant IF/00563/2012 (JGM) and SFRH/BPD/103196/2014 (LA).

A Leading and subleading subjects

The gross features of the differences between the models have been discussed in terms of ΔS_{12} in Sec. 4.1. In this appendix we present the individual z_i distributions only for completeness and with a limited analysis. The distribution of the fraction z_1 of the jet total transverse momentum carried by the leading subjet in jets with $p_T > 150$ GeV/c is shown in Fig. 11 for (top panel) Q-PYTHIA and JEWEL, and (bottom panel) PYQUEN with its three radiation pattern variants. The vacuum references for each model — Q-PYTHIA (vac), JEWEL (vac), and PYTHIA (for PYQUEN) — are also shown. Clearly Q-PYTHIA and JEWEL modify the z_1 distribution in incompatible directions. As noted for ΔS_{12} these observations are consistent with a collimation of jets within JEWEL and broadening in Q-PYTHIA as compared to their vacuum references. For PYQUEN (bottom panel) we find a clear separation of its different parametrisations of the angular distribution of medium induced radiation. The z_2 distribution (the p_T fraction carried by the subleading subjet) shown in Fig. 12 is, by definition, limited to the 0 – 0.5

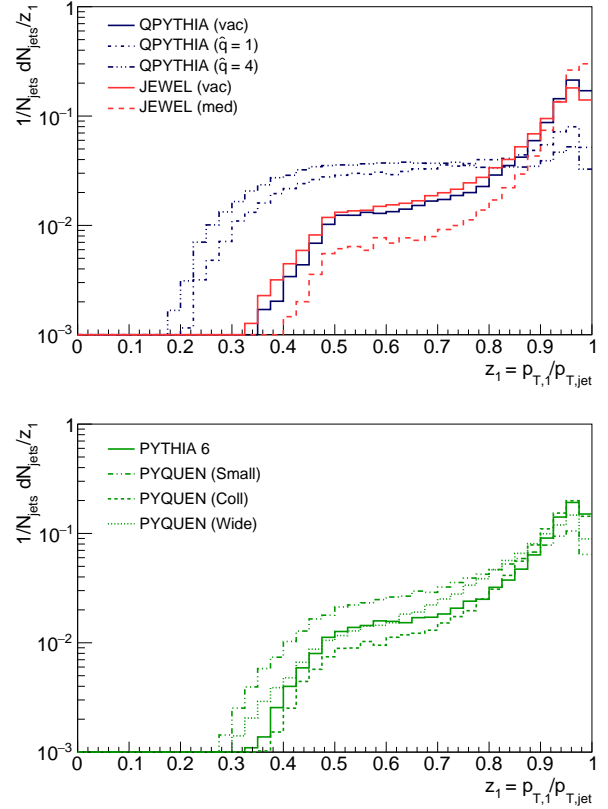


Fig. 11. The fraction of transverse momenta of anti- k_T $R = 0.5$ jets with $p_T > 150$ GeV/c carried by the leading anti- k_T subjet reconstructed with $R_{sj} = 0.15$.

interval. The differences among the z_2 distributions obtained from the different models mirror those observed for z_1 . Globally, the p_T fraction z_2 carried by the subleading subjet reflects the strongly peaked z_1 distribution at large- z which necessarily places the average z_2 to be below 0.1.

References

1. H. Satz, Rept. Prog. Phys. **63**, 1511 (2000). DOI 10.1088/0034-4885/63/9/203
2. S.A. Bass, M. Gyulassy, H. Stoecker, W. Greiner, J. Phys. **G25**, R1 (1999). DOI 10.1088/0954-3899/25/3/013
3. E.V. Shuryak, Phys.Rept. **115**, 151 (1984)
4. J. Cleymans, R. Gavai, E. Suhonen, Phys.Rept. **130**, 217 (1986). DOI 10.1016/0370-1573(86)90169-9
5. J.D. Bjorken, (1982)
6. U.A. Wiedemann, pp. 521–562 (2010). DOI 10.1007/978-3-642-01539-7-17
7. K.M. Burke, et al., Phys. Rev. **C90**(1), 014909 (2014). DOI 10.1103/PhysRevC.90.014909
8. Y. Mehtar-Tani, J.G. Milhano, K. Tywoniuk, Int. J. Mod. Phys. **A28**, 1340013 (2013). DOI 10.1142/S0217751X13400137
9. J. Adams, et al., Nucl.Phys. **A757**, 102 (2005). DOI 10.1016/j.nuclphysa.2005.03.085

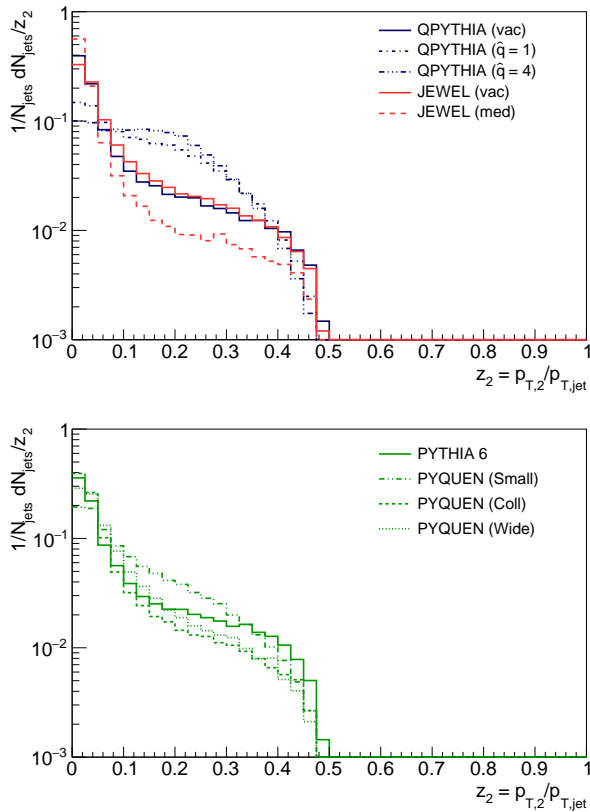


Fig. 12. The fraction of transverse momenta of anti- k_T $R = 0.5$ jets with $p_T > 150$ GeV/ c carried by the subleading anti- k_T subjet reconstructed with $R_{sj} = 0.15$.

10. K. Adcox, et al., Nucl.Phys. **A757**, 184 (2005). DOI 10.1016/j.nuclphysa.2005.03.086
11. I. Arsene, et al., Nucl.Phys. **A757**, 1 (2005). DOI 10.1016/j.nuclphysa.2005.02.130
12. B. Back, et al., Nucl.Phys. **A757**, 28 (2005). DOI 10.1016/j.nuclphysa.2005.03.084
13. K. Aamodt, et al., Phys. Lett. **B696**, 30 (2011). DOI 10.1016/j.physletb.2010.12.020
14. K. Aamodt, et al., Phys. Rev. Lett. **108**, 092301 (2012). DOI 10.1103/PhysRevLett.108.092301
15. S. Chatrchyan, et al., Eur.Phys.J. **C72**, 1945 (2012). DOI 10.1140/epjc/s10052-012-1945-x
16. G. Aad, et al., Phys.Rev.Lett. **105**, 252303 (2010). DOI 10.1103/PhysRevLett.105.252303
17. S. Chatrchyan, et al., Phys.Rev. **C84**, 024906 (2011). DOI 10.1103/PhysRevC.84.024906
18. J. Adam, et al., Phys.Lett. **B746**, 1 (2015). DOI 10.1016/j.physletb.2015.04.039
19. L. Adamczyk, et al., Phys. Rev. **C96**(2), 024905 (2017). DOI 10.1103/PhysRevC.96.024905
20. J. Adam, et al., JHEP **09**, 170 (2015). DOI 10.1007/JHEP09(2015)170
21. G. Aad, et al., Phys.Lett. **B739**, 320 (2014). DOI 10.1016/j.physletb.2014.10.065
22. S. Chatrchyan, et al., Phys.Lett. **B730**, 243 (2014). DOI 10.1016/j.physletb.2014.01.042
23. S. Chatrchyan, et al., JHEP **1210**, 087 (2012). DOI 10.1007/JHEP10(2012)087

24. A.M. Sirunyan, et al., (2017)
25. L. Cunqueiro, Nucl. Phys. **A956**, 593 (2016). DOI 10.1016/j.nuclphysa.2016.02.060
26. M. Rubin, JHEP **05**, 005 (2010). DOI 10.1007/JHEP05(2010)005
27. Z.B. Kang, F. Ringer, W.J. Waalewijn, JHEP **07**, 064 (2017). DOI 10.1007/JHEP07(2017)064
28. A.J. Larkoski, S. Marzani, J. Thaler, Phys. Rev. **D91**(11), 111501 (2015). DOI 10.1103/PhysRevD.91.111501
29. A. Larkoski, S. Marzani, J. Thaler, A. Tripathy, W. Xue, Phys. Rev. Lett. **119**(13), 132003 (2017). DOI 10.1103/PhysRevLett.119.132003
30. C. Frye, A.J. Larkoski, M.D. Schwartz, K. Yan, JHEP **07**, 064 (2016). DOI 10.1007/JHEP07(2016)064
31. S. Marzani, L. Schunk, G. Soyez, JHEP **07**, 132 (2017). DOI 10.1007/JHEP07(2017)132
32. S. Marzani, L. Schunk, G. Soyez, Eur. Phys. J. **C78**(2), 96 (2018). DOI 10.1140/epjc/s10052-018-5579-5
33. C. Collaboration, (2017)
34. M. Aaboud, et al., (2017)
35. X. Zhang, L. Apolinário, J.G. Milhano, M. Ploskon, Nucl. Phys. **A956**, 597 (2016). DOI 10.1016/j.nuclphysa.2016.02.028
36. S. Chatrchyan, et al., JHEP **05**, 090 (2013). DOI 10.1007/JHEP05(2013)090
37. G. Aad, et al., JHEP **05**, 128 (2012). DOI 10.1007/JHEP05(2012)128
38. A. Tripathy, W. Xue, A. Larkoski, S. Marzani, J. Thaler, Phys. Rev. **D96**(7), 074003 (2017). DOI 10.1103/PhysRevD.96.074003
39. K. Kauder, Nucl. Part. Phys. Proc. **289-290**, 137 (2017). DOI 10.1016/j.nuclphysbps.2017.05.028
40. M. Cacciari, G.P. Salam, G. Soyez, JHEP **04**, 063 (2008). DOI 10.1088/1126-6708/2008/04/063
41. M. Cacciari, G.P. Salam, G. Soyez, Eur. Phys. J. **C72**, 1896 (2012). DOI 10.1140/epjc/s10052-012-1896-2
42. B. Abelev, et al., JHEP **1203**, 053 (2012). DOI 10.1007/JHEP03(2012)053
43. M. Cacciari, G.P. Salam, Phys. Lett. **B659**, 119 (2008). DOI 10.1016/j.physletb.2007.09.077
44. N. Armesto, L. Cunqueiro, C.A. Salgado, Eur. Phys. J. **C63**, 679 (2009). DOI 10.1140/epjc/s10052-009-1133-9
45. K.C. Zapp, Eur. Phys. J. **C74**(2), 2762 (2014). DOI 10.1140/epjc/s10052-014-2762-1
46. I.P. Lokhtin, A.M. Snigirev, Eur. Phys. J. **C45**, 211 (2006). DOI 10.1140/epjc/s2005-02426-3
47. T. Sjostrand, S. Mrenna, P.Z. Skands, JHEP **05**, 026 (2006). DOI 10.1088/1126-6708/2006/05/026
48. R. Baier, Y.L. Dokshitzer, A.H. Mueller, S. Peigne, D. Schiff, Nucl.Phys. **B484**, 265 (1997). DOI 10.1016/S0550-3213(96)00581-0
49. A. Dainese, C. Loizides, G. Paic, Eur. Phys. J. **C38**, 461 (2005). DOI 10.1140/epjc/s2004-02077-x
50. L. Apolinario, N. Armesto, L. Cunqueiro, JHEP **02**, 022 (2013). DOI 10.1007/JHEP02(2013)022
51. L.D. Landau, I. Pomeranchuk, Dokl. Akad. Nauk Ser. Fiz. **92**, 535 (1953)
52. A.B. Migdal, Phys. Rev. **103**, 1811 (1956). DOI 10.1103/PhysRev.103.1811
53. K.C. Zapp, Phys. Lett. **B735**, 157 (2014). DOI 10.1016/j.physletb.2014.06.020
54. S.D. Ellis, D.E. Soper, Phys. Rev. **D48**, 3160 (1993). DOI 10.1103/PhysRevD.48.3160

- 55. Y.L. Dokshitzer, G.D. Leder, S. Moretti, B.R. Webber, JHEP **08**, 001 (1997). DOI 10.1088/1126-6708/1997/08/001
- 56. J.G. Milhano, K.C. Zapp, Eur. Phys. J. **C76**(5), 288 (2016). DOI 10.1140/epjc/s10052-016-4130-9
- 57. M. Dasgupta, L. Magnea, G.P. Salam, JHEP **02**, 055 (2008). DOI 10.1088/1126-6708/2008/02/055
- 58. M. Bahr, et al., Eur. Phys. J. **C58**, 639 (2008). DOI 10.1140/epjc/s10052-008-0798-9
- 59. J. Bellm, et al., Eur. Phys. J. **C76**(4), 196 (2016). DOI 10.1140/epjc/s10052-016-4018-8
- 60. B. Andersson, G. Gustafson, G. Ingelman, T. Sjostrand, Phys. Rept. **97**, 31 (1983). DOI 10.1016/0370-1573(83)90080-7
- 61. A. Kupco, pp. 292–300 (1998)
- 62. A. Beraudo, J.G. Milhano, U.A. Wiedemann, Phys. Rev. **C85**, 031901 (2012). DOI 10.1103/PhysRevC.85.031901
- 63. M. Dasgupta, A. Fregoso, S. Marzani, G.P. Salam, JHEP **09**, 029 (2013). DOI 10.1007/JHEP09(2013)029
- 64. A.J. Larkoski, S. Marzani, G. Soyez, J. Thaler, JHEP **05**, 146 (2014). DOI 10.1007/JHEP05(2014)146
- 65. J.G. Milhano, U.A. Wiedemann, K.C. Zapp, (2017). DOI 10.1016/j.physletb.2018.01.029